ORIGINAL PAPER

Submitted: 28.04.2024
Accepted: 12.08.2024
Early publication date:

Endokrynologia Polska
DOI: 10.5603/ep.100459
ISSN 0423–104X, e-ISSN 2299–8306
Volume/Tom 75; Number/Numer 5/2024

Identification of fibrosis-associated lncRNAs in diabetic cardiomyopathy patients

Xiyan Dai[1, 2], Dongping Chen[3], Fan Yang[4], Zhihui Dong[3], Lu Yang[3], Jiading He[5], Jianmin Xiao[1, 3, 5]

[1]*The First Clinical Medical College, Jinan University, Guangzhou, China*
[2]*Department of Comprehensive, Maoming People's Hospital, Maoming, China*
[3]*Central Laboratory, Binhaiwan Central Hospital of Dongguan, Dongguan, China*
[4]*Department of Ultrasound, Binhaiwan Central Hospital of Dongguan, Dongguan, China*
[5]*Department of Cardiology, Binhaiwan Central Hospital of Dongguan, Dongguan, China*

Abstract

Introduction: Our study endeavours to ascertain the plasma-derived long noncoding ribonucleic acids (lncRNA) and messenger RNA (mRNA) expression profiles through gene microarray analysis, aiming to elucidate their potential biological roles in the development and progression of diabetic cardiomyopathy (DCM), particularly with respect to myocardial fibrosis.

Material and methods: We conducted gene chip experiments to discern differences in lncRNA and mRNA expression profiles between diabetic cardiomyopathy and type 2 diabetes mellitus (T2DM). Differentially expressed mRNAs were subjected to functional enrichment analysis, thereby enabling the identification of key genes. Subsequently, we established an interaction network connecting lncRNAs with mRNAs. To validate myocardial fibrosis-related mRNAs, we further developed a rat model of diabetic cardiomyopathy.

Results: We identified 688 differentially expressed lncRNAs and 341 differentially expressed mRNAs, which were primarily enriched in creatine metabolism, small guanosine triphosphate hydrolase (GTPase)-mediated signal transduction, and fatty acid degradation processes. Our analyses revealed 8 core genes (*SMD11*, *DRG1*, *RPS26*, *EIF2S1*, *UBE3A*, *CEBPZ*, *NUP153*, and *EMD*) associated with diabetic cardiomyopathy. An investigation into the lncRNA–mRNA coexpression network underscored 4 lncRNAs (lnc-NEK10-3, lnc-KDM4A-2, lnc-PCYOX1-3, and lnc-CDCP2-1) as significantly linked to differentially expressed fibrosis-associated mRNAs. The expression levels of transmembrane protein 173 (TMEM173) and toll-like receptor 7 (TLR7) were found to be significantly higher in DCM compared to normal controls, whereas cathepsin L1 (CTSL) and forkhead box O3 (FOXO3) displayed significantly lower expression levels relative to those of normal controls.

Conclusions: Our study disclosed a subset of lncRNAs and mRNAs that are implicated in diabetic cardiomyopathy and myocardial fibrosis, thereby presenting themselves as promising biomarkers and therapeutic targets for the management of both diabetic cardiomyopathy and myocardial fibrosis. **(Endokrynol Pol 2024; 75 (5): 525–538)**

Key words: *diabetic cardiomyopathy; myocardial fibrosis; long noncoding RNA; gene chip; bioinformatics*

Introduction

Diabetes mellitus (DM) is a systemic metabolic disorder stemming from the intricate interplay of genetic and environmental elements, characterised by a substantial decline in insulin secretion and a concomitant escalation of blood glucose levels [1]. According to data from the International Diabetes Federation Research Programme, the global prevalence of diabetes among individuals aged 20–79 years reached an estimated 10.5% in 2021, with forecasts suggesting an increase to 12.2% by 2045, affecting approximately 783.2 million people [2]. Cardiovascular complications have emerged as the foremost cause of mortality in DM patients [3], contributing to 44% of deaths in type 1 DM cases and 52% in those with type 2 DM (T2DM) cases [4]. Among the most severe comorbidities is diabetic cardiomyopathy (DCM) [5], where under hyperglycaemic conditions, multiple interconnected detrimental pathways are activated, culminating in cellular damage and tissue inflammation [6]. DCM represents a distinctive cardiac anomaly that develops uniquely in DM patients without concurrent cardiovascular diseases such as coronary artery disease or hypertension. Its hallmark features include myocardial dilation, hypertrophy, reduced diastolic and systolic function of the left ventricle, and eventual progression towards heart failure [7]. In 1954, Lundbaek [8] was one of the pioneers to propose that DCM can develop independently of hypertension and coronary artery disease, often co-existing alongside T2DM. A pivotal pathological characteristic of DCM is myocardial fibrosis, which exacerbates the risk of heart failure, arrhythmias, or even sudden death [9]. Despite extensive research efforts, the intricate pathogenesis underlying both DCM and myocardial fibrosis remains an enigma.

Jianmin Xiao, The First Clinical Medical College, Jinan University, Guangzhou, China; e-mail: xiaojianmin0126@163.com

Long noncoding ribonucleic acids (lncRNAs) represent a class of non-coding RNA molecules characterised by their length exceeding 200 nucleotides and distinctive biological functions, and their emergence through transcription driven by RNA polymerase II [10, 11]. These versatile molecules have demonstrated their ability to regulate gene expression at multiple levels, including transcriptional, post-transcriptional, and post-translational levels, through mechanisms such as guidance, scaffolding, decoying, and signalling [12, 13]. lncRNAs can influence the expression of target genes, whether they are messenger RNA (mRNAs) or microRNAs (miRNAs). For instance, consider lncRNA1/2-sbsRNAs [half staufen1 (STAU1)-binding site RNAs], which engage in paired binding with the Alu element situated in the 3′-untranslated region of mRNA. This pairing forms the binding site for the RNA-binding protein STAU1, thereby promoting its association with mRNA and subsequent degradation through the STAU1-mediated mRNA decay (SMD) pathway [14]. Another instance involves lnc-MD1, which binds to miR-133 and miR-135 through base-complementary pairing, competitively inhibiting their binding to target genes, thereby modulating muscle differentiation [15]. The significance of lncRNAs extends to their involvement in various diseases, including tumours [16, 17], osteoarthritis [18], neurological disorders [19], and cardiovascular diseases [20]. Their involvement in DCM has not gone unnoticed; lncRNAs have been identified as critical regulators in the development and progression of diabetic cardiomyopathy, influencing various cellular processes that contribute to disease onset and progression [21]. For instance, recent research reveals that methyltransferase-like protein 14 (METTL14) suppresses pyroptosis and diabetic cardiomyopathy by decreasing tissue-specific induced non-coding RNA (TINCR) lncRNA expression [22]. Moreover, lncRNA ZNF593-AS has been demonstrated to alleviate diabetic cardiomyopathy by suppressing the interferon regulatory factor 3 (IRF3) signalling pathway [23]. Zhang *et al.* (2016) [24] discovered elevated expression of metastasis-associated lung adenocarcinoma transcript 1 (MALAT1) in the heart, using a rat model of DCM. Cardiac function showed improvement upon MALAT1 knockdown. Additionally, silencing lncRNA-Meg3 yielded a significant reduction in myocardial fibrosis and marked enhancement in cardiac function [25]. However, the journey of plasma lncRNAs during the onset and progression of DCM and myocardial fibrosis, their coexpression patterns with mRNAs, and the underlying regulatory mechanisms warrant further exploration.

In this study, we aimed to delineate the characteristic expression profiles of lncRNAs and mRNAs in the peripheral blood samples derived from patients with T2DM and DCM, using state-of-the-art gene microarray technology. To delve deeper into the functional dimensions of these genetic elements, we harnessed the power of Gene Ontology (GO) and Kyoto Encyclopaedia of Genes and Genomes (KEGG) functional enrichment analyses. We constructed protein–protein interaction (PPI) networks and established lncRNA–mRNA co-expression networks. These multifaceted methodologies played a pivotal role in unravelling the intricate relationship network that interconnects differentially expressed genes (DEGs) and lncRNAs associated with the pathogenesis of DCM and myocardial fibrosis, thereby shedding light on their underlying biological functions. The findings of this study have the potential to introduce novel perspectives and provide invaluable guidance in our quest to comprehend the intricate pathogenesis of DCM and myocardial fibrosis. Furthermore, these results may pave the way for the identification of promising therapeutic targets to address these challenging medical conditions.

Material and methods

General data collection from the study population

We included 5 patients diagnosed with DCM and an additional 5 patients with T2DM, all of whom were hospitalised in the Department of Cardiovascular Medicine at Binhaiwan Central Hospital of Dongguan between September and December 2020. The diagnostic criteria for DCM [26] and T2DM [27] were established based on the existing literature, and all the patients were in compliance of the diagnostic criteria. All patients underwent coronary angiography to rule out coronary artery disease. Exclusion criteria were as follows: (1) hypertensive or acute cerebral infarction; (2) autoimmune diseases; (3) treatment with hormone or immunosuppressant drugs; (4) valve disease; (5) inflammatory or infectious hormonal within 2 weeks before onset of DCM; (6) cardiomyopathy other than DCM; and (7) poor compliance and inability to complete the measurement of the relevant indices. All patients who participated in this study provided signed informed consent.

Laboratory tests and cardiac ultrasound evaluation

Laboratory assessment parameters included blood urea nitrogen (BUN), creatinine, pro-brain natriuretic peptide (BNP), and glycated haemoglobin (HBA_{1c}). Cardiac ultrasound evaluation parameters were as follows: left ventricular end-diastolic internal diameter (LVIDd), left ventricular end-systolic internal diameter (LVIDs), fractional shortening (FS), and left ventricular ejection fraction (LVEF).

Overnight blood collection, total RNA quantification, quality control, and gene chip testing

Peripheral blood samples (5 mL) were collected from participants in ethylenediaminetetraacetic acid (EDTA) tubes. Plasma was isolated by centrifugation at 3000 × g for 15 min at 4°C and stored at −80°C. The total RNA was quantified by NanoDrop ND-2000 (Thermo Scientific), and RNA integrity was assessed using Agilent Bioanalyzer 2100. Subsequently, the total RNA was reverse transcribed into

double-stranded complementary deoxyribonucleic acid (cDNA), followed by cRNA synthesis. A second cycle cDNA was synthesised from cRNA. Following fragmentation and biotin labelling, second cycle cDNA was hybridised onto the microarray. After washing and staining, the arrays were scanned by an Affymetrix Scanner 3000. The Affymetrix oelnc microarray experiments were performed by OE Biotechnology Co. Ltd. (Shanghai, China).

Data quality control

Chip Scan

The raw data scan graph of the Affymetrix chip was mainly used to show how well each sample was scanned, such as whether the scan was even and whether there were any large scratches. The chip was labelled with biotin, which was displayed as a grey-scale plot on the scan graph. Each point on the graph corresponds to a probe (Supplementary File — Figure S1).

Outlier detection

The boxplot method was used to identify extreme data points. The dataset was divided into quartiles with Q1 and Q3 representing the lower and upper quartiles, respectively, while the interquartile range (IQR) was calculated as the difference between these 2 values. Data points lying outside the range of Q1 – 1.5 × IQR to Q3 + 1.5 × IQR were classified as outliers. This widely accepted statistical approach effectively detects observations that significantly deviate from the central tendency of the data. Detailed information can be found in Supplementary File — Figure S2.

Data analysis

Affymetrix Gene Chip Command Console (version 4.0) software was used to extract raw data. Expression Console version 1.3.1 (Affymetrix) software provided robust multiarray averaging (RMA) normalisation for both gene and exon level analysis.

Bioinformatics analysis

Differential gene expression analyses

The differential gene expression analysis was conducted using Genespring software version 14.9, provided by Agilent Technologies. DEGs were screened using t-test p values and fold change values, and the criteria for screening were up- or downregulated fold change ≥ 2.0 and $p \leq 0.05$. To discern the primary biological functions and pathways influenced by the differentially expressed mRNAs, GO and KEGG enrichment analyses were carried out. Ultimately, unsupervised hierarchical clustering analysis and volcano plots were generated to visually represent the distinctive expression patterns among various samples.

Construction of PPI networks and identification of core genes for DEGs

The PPI networks between DEGs were evaluated using String software version 1.0.0. Node data of interactions with a composite score > 0.4 obtained from String were imported into Cytoscape software version 3.10.0 for analysis. The top 15 focus genes were obtained by applying the cytoHubba plug-in in Cytoscape software using the maximal clique centrality (MCC), maximum neighborhood component (MNC), and density of maximum neighborhood component (DMNC) algorithms, respectively, and the core genes were obtained by intersection after plotting the Venn diagrams.

Analysis of mRNA and lncRNA coexpression

Based on related literature and functional enrichment results of the differentially expressed mRNAs, 4 transcripts associated with myocardial fibrosis were selectively analysed. Pearson correlation analysis was used to quantify the associations between these myocardial fibrosis-related mRNAs and all differentially expressed lncRNAs detected in the plasma samples of the 10 subjects. A stringent threshold was set in the correlation analysis, where the absolute value of the correlation coefficient had to be ≥ 0.80 and the p-value ≤ 0.05. With these criteria, the significant mRNA-lncRNA interaction pairs were systematically screened.

Reverse transcription, quantitative real-time polymerase chain reaction (RT-qPCR)

A miRcute Serum/Plasma miRNA Isolation kit (1608, Tiangen) was utilised to extract exosomal total RNA from plasma samples of patients with proto-DCM and T2DM, to verify the expression levels of myocardial fibrosis-related lncRNAs. The PrimeScript RT reagent Kit (Perfect Real Time) (RR047A, Takara) was utilised to reverse transcribe RNA into cDNA. The expression level of lncRNAs was assessed through RT-qPCR with Universal SYBR qPCR Master Mix (BL697A, Biosharp). The relative expression of the target gene was determined using the $2^{-\Delta\Delta Ct}$ method. Primer sequences are detailed Table 1.

Rat DCM model establishment

A group of 20 male rats, each 7 weeks old, were purchased from SPF Biotechnology (SPF, Beijing, China). Each rat was maintained in an environment free of specific pathogens (with a temperature range of 21–25°C and humidity between 50 and 70%) following a 12-hour light/dark cycle. Each animal experiment followed the protocols approved by the Medical Ethics Committee of the Jinan University. The rats were randomly allocated into 2 distinct experimental categories: one group served as the healthy control (CON), while the other was designated as the DCM group. The DCM group of rats received an intraperitoneal injection of 1% streptozotocin (S817944, Macklin, China) at a dose

Table 1. *Polymerase chain reaction (PCR) primer list*

	Forward (5'-3')	Reverse (5'-3')
lnc-NEK10-3	CAGTTCTCCTGCCTCAGCCTCT	TGAGACCAGCCTTGCCAACATG
lnc-CDCP2-1	CCATCTCAGCTCACTGCAACCT	TGAGGCAGGCGGATCACTTGA
lnc-PCYOX1-3	ATGTTGCCCAGGCTAGTCTTGAAC	AGGCTAGAGTGCAGTGGTGTGAT
lnc-KDM4A-2	CTCACTGCAACCTCCACCTCCT	CAAGACGAGCCTGGGCAAACAT
TMEM173	ACCACCAAGTCACACTCT	GACCAGGATGCCAAGATG
CTSL	GGAAGAGTGGAGGAGAGCAGTGT	GTCATGTCACCGAAGGCGTTCAT
FOXO3	AGGCTCCTCACTGTATTCA	TTCGCTACGGATGATGGA
TLR7	GTTCTTGACCTTGGCACTA	CAACTTCTCTTGACTCTTCTG

of 70 mg/kg/dose over a period of 5 days to impair pancreatic beta-cell activity. In the CON group, rats received an intraperitoneal injection of a comparable amount of sodium citrate buffer. One week after the streptozotocin (STZ) injection, blood was collected from the tail vein of the rats to assess their fasting blood glucose levels. The DCM rat model was established when blood glucose exceeded 16.7 mmol/L and the rats exhibited symptoms of irritable thirst, excessive eating, and frequent urination [28]. The echocardiographic test was performed after a period of 16 weeks.

Rat echocardiography

The rats underwent anaesthesia using 2% phenobarbital, and at 16 weeks, transthoracic M-mode echocardiography was conducted using the L15-7io probe (Ultrasound Transducer Bossel, WA 98021, USA). Measurements were taken for these metrics: left ventricular ejection fraction (EF%), left ventricular shortening fraction (FS%), systolic and diastolic internal dimensions of the left ventricle (LVIDs and wall LVIDd), and cardiac output (CO).

Masson's trichrome staining

Hearts fixed in 4% paraformaldehyde were embedded in paraffin, sectioned at 5 μm thickness, and subjected to Masson's trichrome staining to assess the severity of myocardial fibrosis. Microscopic analysis of the stained heart sections revealed collagen accumulations, which were marked as blue-stained regions, indicating fibrosis.

RT-qPCR and western blotting (WB)

Total RNA was isolated from rat hearts using TRIzol reagent and extracted using the Tiangen kit (DP419, Tiangen, China). After measuring the corresponding concentrations, the RNA samples were reverse transcribed into complementary DNA (cDNA). Finally, RT-qPCR was performed to verify the expression level. The reverse transcription and qPCR kits and methods were as described previously, and primer sequences are listed in Table 1.

Methods of WB: Total proteins from cardiac tissues were extracted with RIPA lysis buffer (P0013B, Beyotime, China) containing protease inhibitors (P0100, Solarbio, China). Protein concentrations were quantified using a bicinchoninic acid (BCA) protein assay kit (BL521A, Biosharp, China). Equal amounts of proteins were first separated by 10% sodium dodecyl sulphate–polyacrylamide gel electrophoresis (SDS-PAGE) and then transferred to a polyvinylidene (PVDF) membrane (Millipore, USA). After sealing with 5% skimmed milk for 2 h at room temperature, the membranes were washed and incubated overnight with the following primary antibodies: toll-like receptor 7 (TLR7) 1:1000, forkhead box O3 (FOXO3) 1:1000, Wanleibio, cathepsin L1 (CTSL) 1:1000, transmembrane protein 173 (TMEM173) 1:5000, Proteintech, China. It was washed with TBST and then incubated with the appropriate horseradish peroxidase (HRP)-conjugated secondary antibody (ab205718, Abcam, UK, FDM007, FUDE, China) for 1 h at room temperature. The target bands were then detected using a chemiluminescence (ECL) kit (KF8001, Affinity, China). β-Tubulin (1:5000, FUDE, China) was used as a reference for total cellular proteins. Signal density was quantified using ImageJ.

Statistical analysis

All data were subjected to statistical analysis utilising GraphPad Prism version 8.0 software. For the comparison of 2 sets of data, either Student's t-test or the non-parametric Mann-Whitney U test was employed, as appropriate. Two-way ANOVA was used for the 2 multivariate data analyses. Statistical significance was established at a 2-tailed p-value less than 0.05.

Results

Baseline characteristics and blood parameters assessment

The baseline information revealed that the DCM group had a significantly lower mean age compared to the T2DM group ($p = 0.032$, Tab. 2). The 2 groups have significantly different cardiac functional grading. In terms of blood analyses, it was observed that the levels of N-terminal pro-B-type natriuretic peptide (NT-pro-BNP) were significantly elevated in the DCM group relative to the control group ($p < 0.05$). However, there were no statistically significant differences between the 2 groups regarding gender, duration of diabetes, HBA_{1c}, BUN, and creatinine concentrations ($p > 0.05$).

Echocardiographic parameters in the study population

Comparative analysis revealed that, compared with the T2DM group, left ventricular end-diastolic internal diameter (LVEDd) and left ventricular end-systolic internal diameter (LVEDs) were significantly higher in the DCM group ($p < 0.05$). Conversely, LVEF and left ventricular FS were notably lower in the DCM group as opposed to the T2DM group ($p < 0.05$) (Fig. 1).

Table 2. *Basic information and blood analysis*

Basic information	DCM (n = 5)	T2DM (n = 5)	p-value
Age [years]	56.4 ± 9.02	67.8 ± 7.20	0.032
Male/female [case]	3/2	1/4	0.52
Duration of diabetes [years]	5.8 ± 1.48	5.6 ± 1.52	0.838
Cardiac functional grading	3.0(0.50)	1(0)	0.008
HBA_{1c}(%)	8.8 ± 2.0	7.4 ± 0.5	0.204
BUN [mmol/L]	6.0 ± 1.9	6.0 ± 2.9	0.988
Cr [umol/L]	88.8 ± 36.5	74.0 ± 14.2	0.841
NT-proBNP [pg/mL]	11104.7 ± 13474.8	50.0 ± 6.2	0.008

HBA_{1c} — haemoglobin A1c; BUN — blood urea nitrogen; Cr — creatinine; NT-pro-BNP — N-terminal pro-brain natriuretic peptide

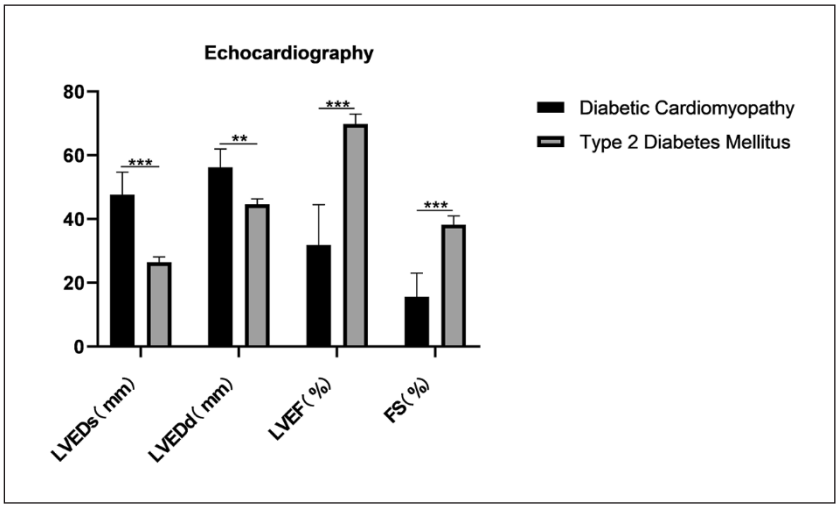

Figure 1. *Echocardiography in patients with diabetic cardiomyopathy (DCM) and type 2 diabetes mellitus (T2DM). LVEDs — left ventricular end-systolic diameter; LVEDd — left ventricular end-diastolic diameter; LVEF — left ventricular ejection fraction; FS — fractional shortening. Data are represented as mean ± standard error of the mean (SEM), ***p < 0.001, **p < 0.005. Differentially expressed mRNAs in peripheral blood of T2DM and DCM patients*

The mRNA expression profiles from gene chip analysis in both T2DM and DCM groups are depicted in Figure 2. The hierarchical clustering heatmap clearly illustrates that there is a significant divergence in mRNA expression patterns between patients with DCM and control subjects (Fig. 2A). The volcano

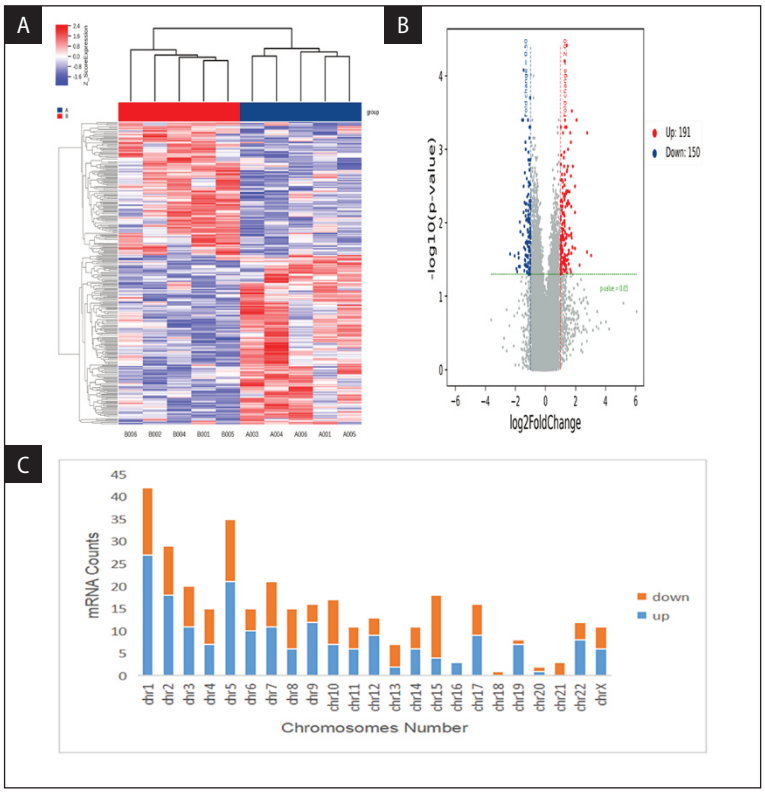

Figure 2. *Messenger ribonucleic acid (mRNA) expression profiles in patients with diabetic cardiomyopathy (DCM).* **A.** *Hierarchical cluster analysis showing mRNAs differentially expressed between DCM and control groups. Red and blue colours represent up- and downregulated mRNAs with > 2-fold changes;* **B.** *Volcano plots showing mRNAs differentially expressed in patients with DCM compared with controls. Red and blue dots represent up- and downregulated mRNAs, respectively. The horizontal green line indicates *p ≤ 0.05, while vertical red and blue lines indicate up- and downregulated twofold changes, respectively;* **C.** *Chromosomal distribution of mRNAs dysregulated in DCM. DCM, diabetic cardiomyopathy*

plots from the differential expression analysis show that 341 mRNAs were differentially expressed in the DCM group, out of which 191 were upregulated and 150 were downregulated (Fig. 2B). Notably, chromosome 1 harboured the highest number of deregulated mRNAs in DCM patients relative to controls (Fig. 2C).

Differentially expressed lncRNAs in peripheral blood of DM and DCM patients

The lncRNA expression profiles in the peripheral blood of DCM patients are shown in Figure 3, and the difference between the DCM and T2DM groups was significant ($p < 0.05$). The regulatory profiles of lncRNAs were significantly different between DCM patients, as shown in the heat map of hierarchical cluster analysis (Fig. 3A). Relative to the control group, 688 lncRNAs exhibited altered expression levels in the DCM group, with 635 being upregulated and 53 downregulated, as illustrated in the volcano plot (Fig. 3B). In DCM patients, chromosome 1 had the largest number of deregulated lncRNAs compared with the controls (Fig. 3C).

Functional enrichment analysis of differentially expressed mRNAs

Figure 4 presents the outcomes of GO and KEGG pathway enrichment analysis conducted on 341 differentially expressed mRNAs. The top 10 most significant GO entries for biological processes, cellular components, and molecular functions are visually represented as bar plots. The upregulated mRNAs were mainly involved in biological processes such as creatine metabolism (GO: 0006600), lipoprotein transport (GO: 0042953), and respiratory gaseous exchange (GO: 0007585). Within the cellular component category, these upregulated transcripts were predominantly localised to the integrative component of the endoplasmic reticulum membrane (GO: 0030176), the endoplasmic reticulum membrane itself (GO: 0005789), and polysomes (GO: 0005844). At the molecular functional level, they were mainly involved in myosin light chain binding (GO: 0032027), transcription coactivator activity (GO: 0003713), and lipid binding (GO: 0008289) (Fig. 4A). The downregulated mRNAs were predominantly implicated in the biological processes of small GTPase-mediated

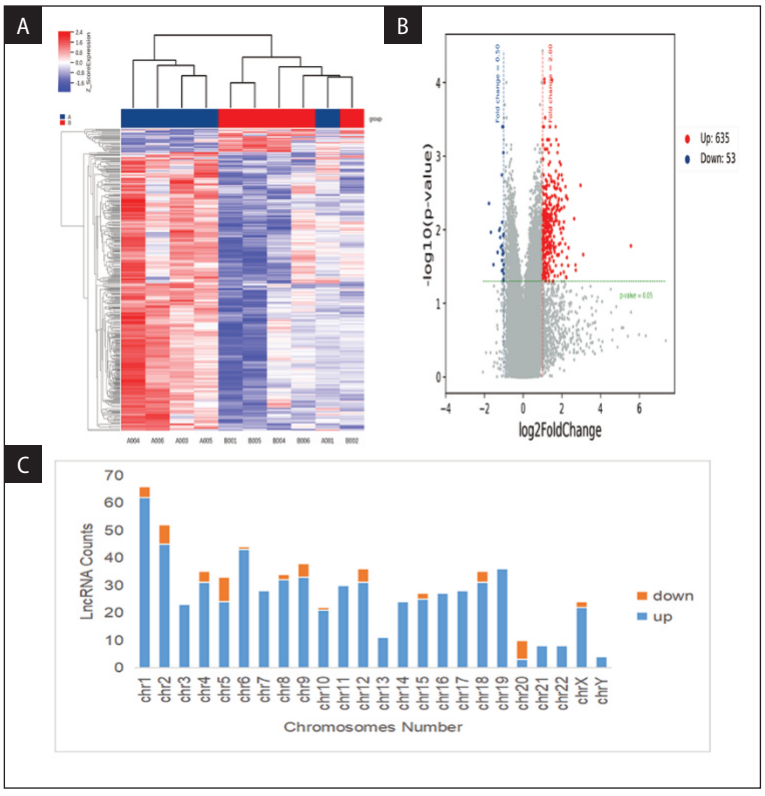

Figure 3. *Long noncoding ribonucleic acids (lncRNA) expression profiles of diabetic cardiomyopathy (DCM) patients.* **A.** *Hierarchical cluster analysis showing lncRNAs differentially expressed between DCM and control groups. Red and blue colours represent up- and downregulated lncRNAs with > 2-fold change, respectively;* **B.** *Volcano plots showing lncRNAs differentially expressed in patients with DCM compared with controls. Red and blue dots represent up- and downregulated lcRNAs, respectively. The horizontal green line indicates *p ≤ 0.05, while vertical red and blue lines indicate up- and downregulated twofold changes, respectively;* **C.** *Chromosomal distribution of lncRNAs dysregulated in DCM*

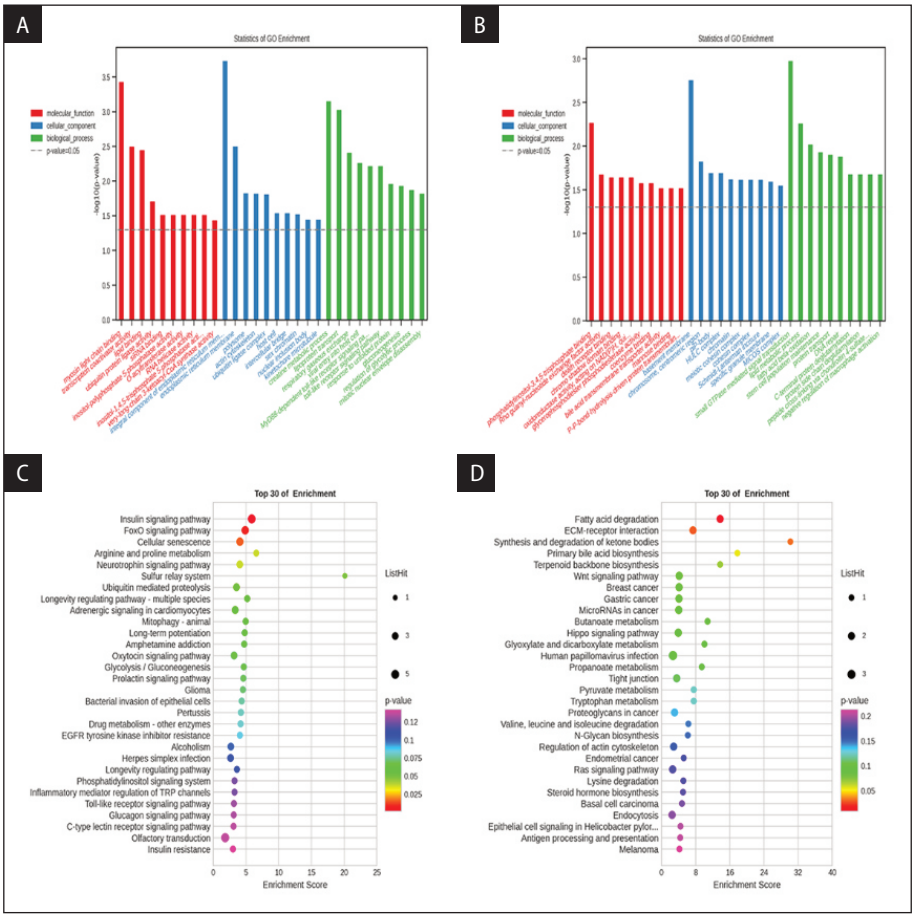

Figure 4. *GO and KEGG term enrichment analysis of DEGs.* **AB.** *The 10 most significant GO entries with upregulated and downregulated differentiated mRNAs,. The y-axis shows -log10 (p) value. The higher the bar, the lower the corresponding p value. Different color distributions correspond to biological process, cellular component, and molecular function;* **CD.** *KEGG pathway analysis of upregulated and downregulated differential mRNAs. the x-axis represents the degree of enrichment and the y-axis the pathway of enrichment. The larger the dot in the figure, the more genes fall into that pathway and the color of the bubble changes from purple to blue, green and red, and the smaller the enrichment p value, the greater the significance. DEG — differentially expressed gene; GO — Gene Ontology; KEGG — Kyoto Encyclopedia of Genes and Genomes*

signal transduction, as characterised by GO term GO:0007264, lipid metabolism (GO: 0006629), and fatty acid beta-oxidation (GO: 0006635). In terms of cellular compartments, these downregulated genes were particularly concentrated within the basement membrane (GO: 0005604), the centromeric region of chromosomes (GO: 0000775), and piP-bodies (GO: 0071547). At the molecular functional level, they were mainly involved in phosphatidylinositol-3,4,5-trisphosphate binding (GO: 0005547), Rho guanyl-nucleotide exchange factor activity (GO:0005089), death receptor binding (GO: 0005123), and other functions (Fig. 4B). The upregulated DEGs were mainly associated with signalling pathways such as insulin signalling (hsa04910), FoxO signalling (hsa04068), and cellular senescence (hsa04218) (Fig. 4C). The downregulated DEGs were mainly involved in fatty acid degradation (hsa00071), extracellular matrix (ECM)–receptor interaction (hsa04512), and synthesis and degradation of ketone bodies (hsa00072) (Fig. 4D).

Construction of the PPI network and screening of core genes

The obtained differentially expressed mRNAs were imported into String online analysis software to obtain the differential gene PPI network graph consisting of 190 nodes and 99 edges (Fig. 5A). Subsequently, these data were imported into Cytoscape software to identify the overlapping genes as core genes according to the 3 sequencing methods obtained in cytoHubba plug-in (Fig. 5B). Through this process, we obtained *PSMD11*, *DRG1*, *RPS26*, *EIF2S1*, *UBE3A*, *CEBPZ*, *NUP153*, and *EMD* key genes as the core genes of diabetic cardiomyopathy.

Coexpression analysis of mRNAs and lncRNAs

Associations between myocardial-fibrosis-related mRNAs (TMEM173, CTSL, FOXO3, TLR7) and differentially expressed lncRNAs were determined by Pearson correlation analysis. This analysis yielded

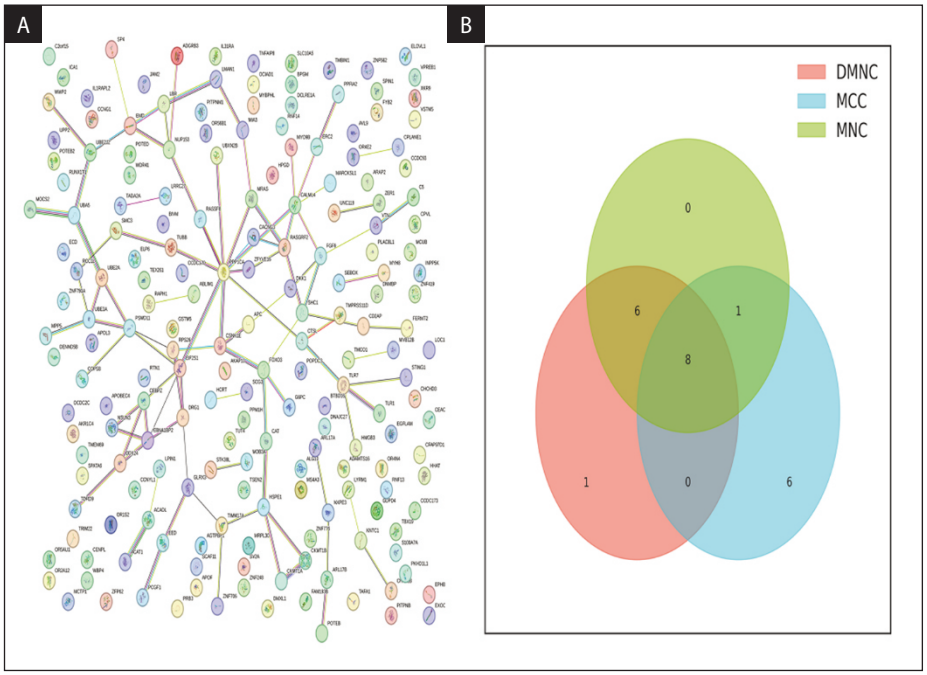

Figure 5. *Diagram of the protein–protein interaction (PPI) network and Venn diagram.* **A.** *Gene PPI network;* **B.** *Venn diagram of core genes obtained using maximal clique centrality (MCC), maximum neighborhood component (MNC), and density of maximum neighborhood component (DMNC) algorithms*

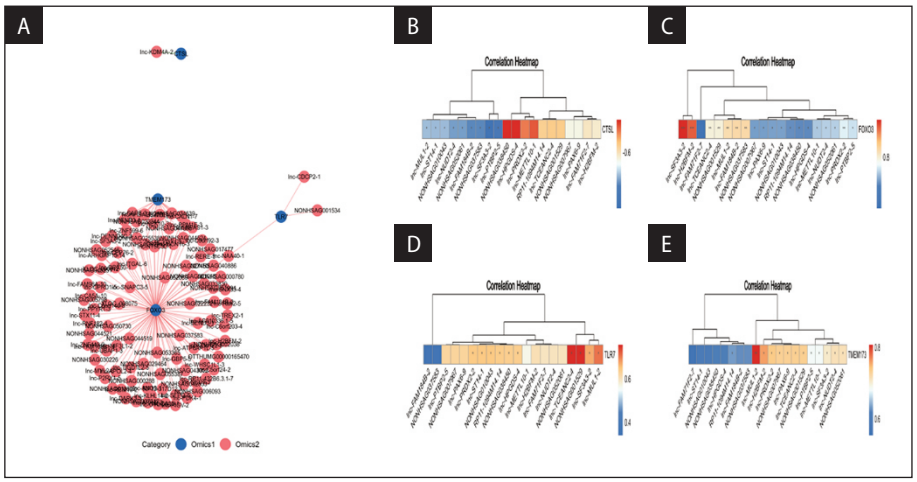

Figure 6. *Coexpression analysis of fibrosis-related messenger ribonucleic acids (mRNAs) with long noncoding RNAs (lncRNAs).* **A.** *Network diagram of fibrosis-related mRNAs coexpressed with lncRNAs. Blue circles represent coexpressed mRNAs, red circles represent coexpressed lncRNAs, the red line represents positive correlation, and the green line represents negative correlation;* **B–E.** *Heatmap of coexpression clustering of cathepsin L1 (CTSL), forkhead box O3 (FOXO3), toll-like receptor 7 (TLR7), and transmembrane protein 173 (TMEM173) with differential lncRNAs. The vertical axis is mRNA and the horizontal axis is lncRNA*

a total of 121 pairs of mRNA–lncRNA relationships (Fig. 6).

Validation of fibrosis-associated mRNAs and lncRNAs by RT-qPCR

To validate the gene chip data, we employed RT-qPCR to assess the expression levels of 4 fibrosis-related lncRNAs in plasma samples from individuals diagnosed with DCM and T2DM. The RT-qPCR results confirmed that the expression levels of certain lncRNAs, including lnc-NEK10-3, lnc-CDCP2-1, and lnc-PCYOX1-3, were significantly upregulated in the plasma of DCM patients. Conversely, the expression level of lnc-KDM4A-2 was found to be decreased in the plasma of these pa-

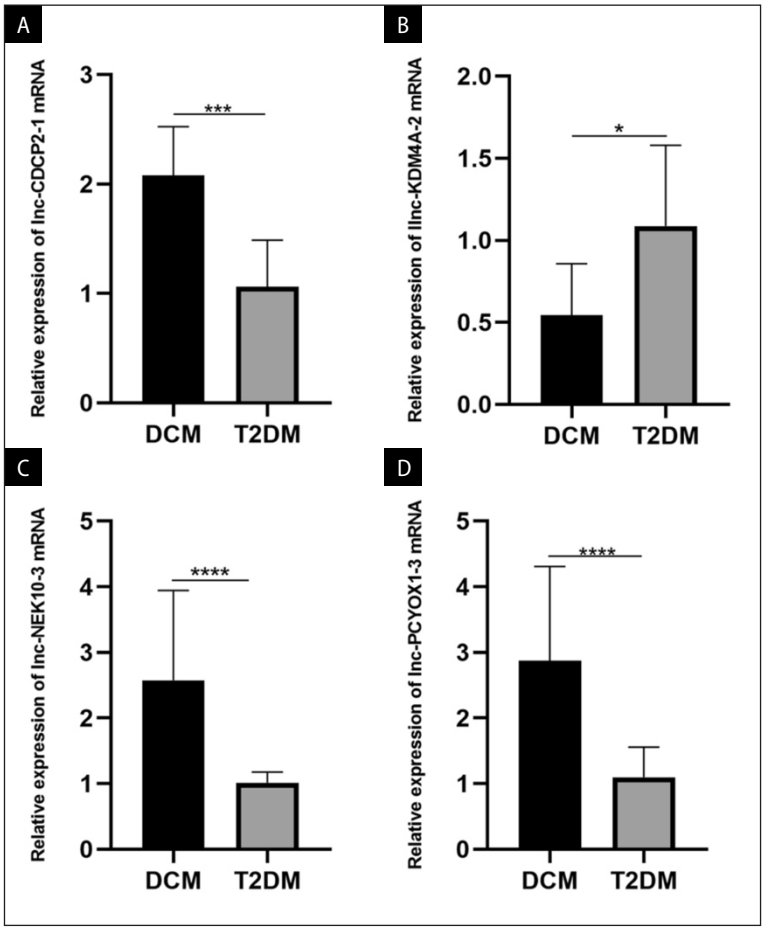

Figure 7. *Validation of long noncoding ribonucleic acids (lncRNAs) was performed using reverse transcription, quantitative real-time polymerase chain reaction (RT-qPCR) analysis. The expression of each lncRNA was normalised to that of U6.* **A–D.** *The gene expression levels of lnc-CDCP2-1, lnc-KDM4A-2, lnc-NEK10-3 and lnc-PCYOX1-3, respectively. Data are presented as mean ± standard error of the mean (SEM). Statistical significance was indicated as *p < 0.05 and **p < 0.005*

tients (Fig. 7). These RT-qPCR findings concurred with the original gene chip data, thereby authenticating the expression patterns observed earlier.

Characterisation of rats with STZ-induced diabetic cardiomyopathy

A total of 8 rats were included in this study, consisting of 4 rats with DCM and 4 control (CON) rats. Relative to the CON rats, the DCM rats displayed significantly elevated blood glucose levels and reduced body weight (Fig. 8AB). Echocardiographic results showed significant cardiac enlargement and decreased EF and FS in the DCM rats compared to the CON rats (Fig. 8C), suggesting systolic and diastolic dysfunction in the DCM rats. Masson trichrome staining showed a significant increase in myocardial fibrosis in the DCM rats (Fig. 8D).

Validation of relative gene expression levels and protein levels of fibrosis-related genes

Compared with the CON group, the gene expression and protein levels of TMEM173 and TLR7 were increased in DCM group rats (Fig. 9ADE), while the gene expression and protein levels of CTSL and FOXO3 were significantly decreased (Fig. 9BCE).

Discussion

This study used gene microarray technology to analyse blood samples from DCM and T2DM patients, discovering 4 lncRNAs strongly linked with myocardial fibrosis mRNAs via bioinformatics screening and experimental validation. These lncRNAs are believed to regulate fibrosis progression in DCM, providing novel insights into disease mechanisms and potential therapeutic targets for cardiac fibrosis.

The clinicopathological phenotype of DCM is prominently characterised by several distinguishing attributes, such as myocardial fibrosis, ventricular dilation, and cardiac dysfunction, all of which can culminate in heart failure [29, 30]. In our study, NT-pro-BNP, a biomarker reflecting heart failure status, was observed to be significantly elevated in the DCM patient group.

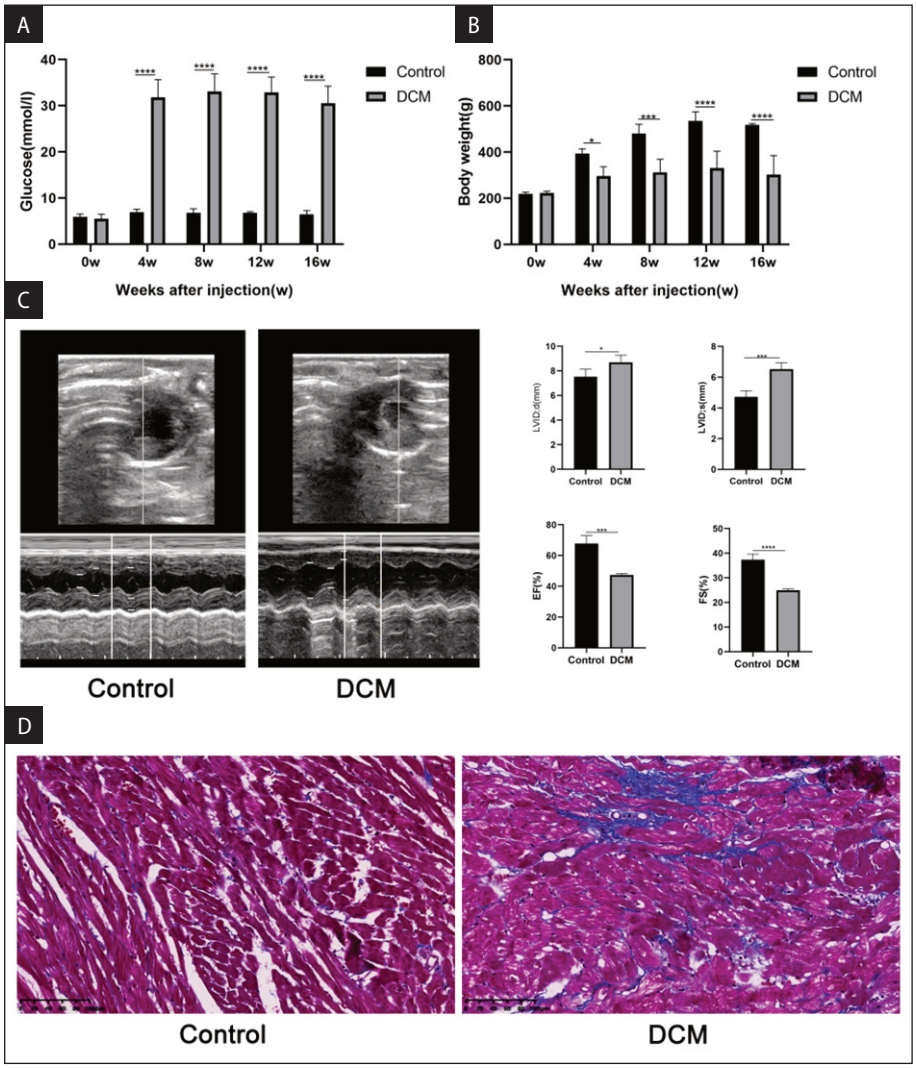

Figure 8. *Characterisation of streptozotocin (STZ)-induced diabetic cardiomyopathy in rats.* **A.** *Fasting blood glucose levels of rats in the diabetic cardiomyopathy (DCM) and control (CON) groups;* **B.** *Body weight of rats in the DCM and CON groups;* **C.** *Heart ultrasound results for DCM and CON rats;* **D.** *Results of Masson's trichrome staining of myocardial tissue in both groups. The results showed a significant increase in myocardial fibrosis in DCM. Data are represented as mean ± standard error of the mean (SEM),****$p < 0.0001$,***$p < 0.001$,**$p < 0.005$. LVEDd — left ventricular end-diastolic diameter; LVEDs — left ventricular end-systolic diameter; LVEF — left ventricular ejection fraction; FS — fractional shortening*

Moreover, cardiac ultrasonography findings indicated substantial cardiac enlargement, significantly decreased ejection fractions, and reduced transient shortening rates in the left ventricle. The clinical features in all the enrolled patients were basically in line with those of DCM.

Despite the surge in research interest and the wealth of studies focusing on DCM during the last decade, the molecular underpinnings driving its onset and progression remain only partially elucidated. As molecular biology has advanced, gene microarray technology has become a valuable tool for gaining insights into complex diseases, including DCM [31, 32]. In the present work, we employed gene microarray technology to identify differentially expressed lncRNAs and mRNAs in the peripheral blood samples of individuals diagnosed with both DCM and T2DM. Furthermore, we used GO and KEGG functional enrichment analyses to expound upon the biological functions of the identified differentially expressed mRNAs. Additionally, we constructed a PPI network to sieve out core genes, and we assembled a coexpression network pertaining to fibrosis-associated lncRNAs and mRNAs.

This study disclosed discernible differences in the plasma expression levels of lncRNAs and mRNAs between individuals afflicted with DCM and those with T2DM. The analytical process pinpointed a total of 688 differentially expressed lncRNAs and 341 DEGs. Among these, 635 differentially expressed lncRNAs were upregulated, while 53 were downregulated. Additionally, 191

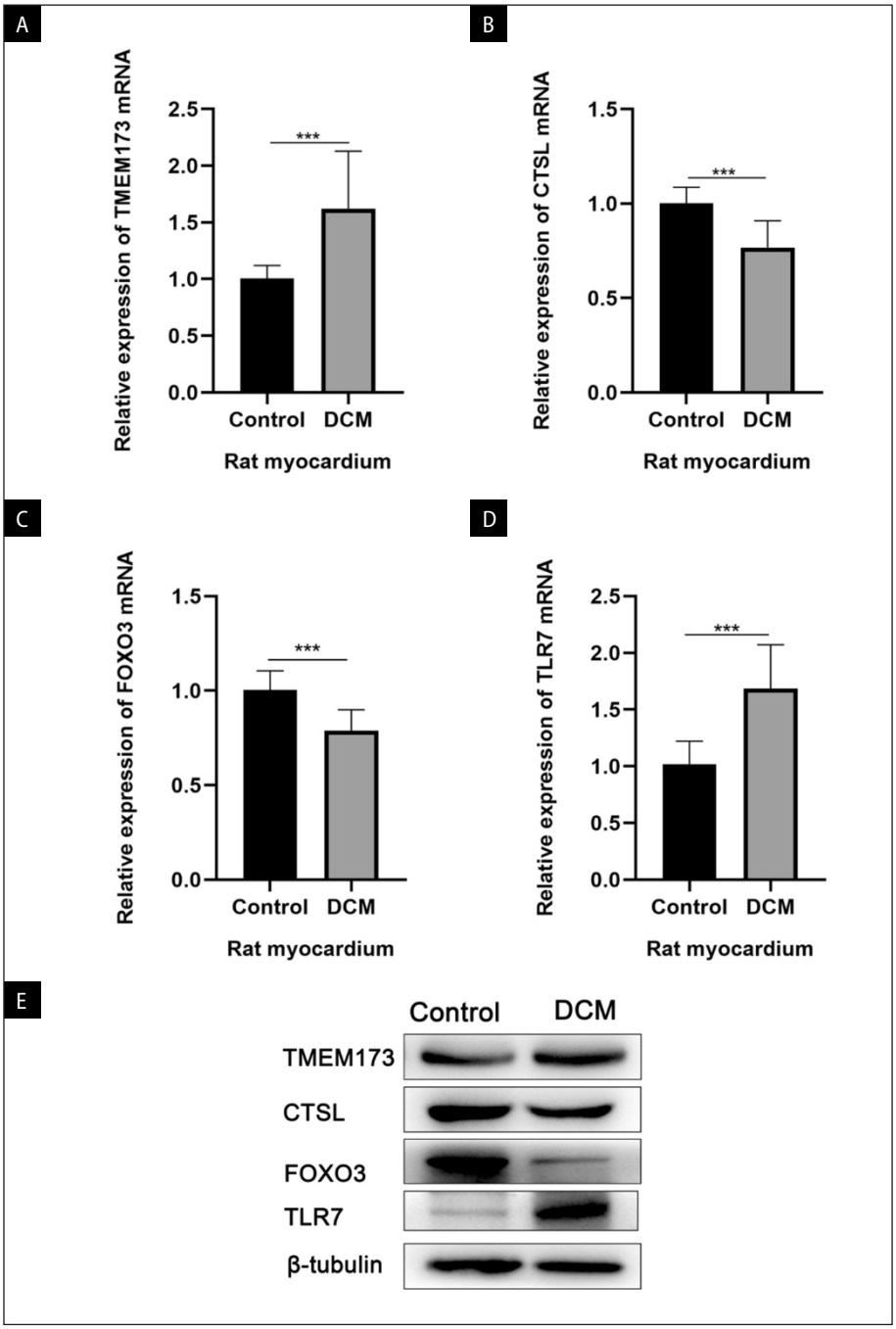

Figure 9. *Relative expression and protein levels of fibrosis genes.* **A–D.** *Gene expression levels of transmembrane protein 173 (TMEM173), cathepsin L1 (CTSL), forkhead box O3 (FOXO3) and toll-like receptor 7 (TLR7), respectively;* **E.** *Protein expression levels of TMEM173, CTSL, FOXO3, and TLR7, respectively. Data are represented as mean ± standard error of the mean (SEM), *** $p < 0.001$*

DEGs were upregulated and 150 were downregulated. Scrutiny of our transcriptomic data exposed that the aberrantly expressed lncRNAs and mRNAs were predominantly localised on chromosome 1. Several studies have previously established a connection between DM and DCM with genetic predisposition factors [33–35]. Thus, chromosome 1 may harbour lncRNAs and mRNAs that confer a heightened risk for developing DCM.

Subsequently, we conducted a comprehensive bioinformatics analysis on the DEGs identified in peripheral blood samples. GO analysis indicated that the most significantly enriched entries of upregulated DEGs were creatine metabolism (GO: 0006600), an integral component of endoplasmic reticulum membrane (GO: 0030176), and myosin light chain binding (GO: 0032027). KEGG pathway enrichment of upregulated DEGs showed insulin signalling pathway (hsa04910), FoxO signalling pathway (hsa04068), cellular senescence (hsa04218), and other pathways. The downregulated DEGs were mainly enriched in the lipid metabolic process (GO: 0006629),

basement membrane (GO: 0005604), and phosphatidylinositol-3,4,5-trisphosphate binding (GO: 0005547). Downregulation of the DEG KEGG enrichment was shown to be mainly involved in signalling pathways such as fatty acid degradation (hsa00071), ECM–receptor interaction (hsa04512), synthesis and degradation of ketone bodies (hsa00072), and other signalling pathways. Previous research has established that creatine metabolism is implicated in myocardial ischaemia-reperfusion injury in T2DM [36] and the onset and progression of DCM [37]. Myosin light chain binding has been shown to correlate with left ventricular systolic dysfunction specific to DCM [38], while lipid metabolic processes are linked to the pathogenic mechanisms of DCM [39]. Basement membrane alterations are associated with the thickening of capillary basement membranes in DCM [40, 41]. A multitude of studies have demonstrated the insulin signalling pathway's involvement in DCM development and progression [42–46]. Cellular senescence plays a role in diabetic cell aging [47], while fatty acid degradation contributes to mitochondrial dysfunction in DCM. ECM–receptor interaction is involved in the development of diabetic nephropathy [48]. Synthesis and degradation of ketone bodies are associated with diabetic cardiac energy efficiency and diabetic heart failure [49]. Therefore, we hypothesise that these distinctive mRNAs in the peripheral blood may contribute to the pathogenesis of DCM through the various pathways described above. Moreover, we identified 8 critical genes (*SMD11*, *DRG1*, *RPS26*, *EIF2S1*, *UBE3A*, *CEBPZ*, *NUP153*, *EMD*) within the peripheral blood DEGs through construction of a protein-protein interaction (PPI) network and examination of a Venn diagram. These genes might play a crucial role in the pathological mechanisms underlying DCM.

We systematically screened and selected 4 mRNAs (TMEM173, CTSL, FOXO3, and TLR7) that have documented associations with myocardial fibrosis, following extensive literature review and differential mRNA function enrichment analysis. To validate the roles of these mRNAs, we utilised a DCM rat model. Our constructed DCM rat model confirmed that diabetes-induced conditions led to significant cardiac dilation and myocardial fibrosis, aligning with previous research findings [50]. Our experimental results revealed that in the DCM rats, compared to their normal counterparts, the expression levels of TMEM173 and TLR7 were significantly elevated, as verified through RT-qPCR and western blot analysis. Conversely, the expression levels of CTSL and FOXO3 were significantly diminished. Previous studies have shed light on the involvement of these mRNAs in myocardial fibrosis. For instance, stimulator of interferon genes 1 (STING1) signalling, which regulates autophagy and multiple cell death pathways including pyroptosis, is implicated in both health maintenance and disease progression, particularly with respect to its close connection to the advancement of dilated cardiomyopathy (DCM) [51, 52]. Furthermore, inhibiting or knocking down TMEM173, commonly known as STING, has been shown to ameliorate cardiac hypertrophy in DCM mouse models [53]. Histone-L (CTSL) has been demonstrated to enhance cardiac function by suppressing cardiac hypertrophy, inflammation, and fibrosis via the inhibition of the protein kinase B/glycogen synthase kinase 3 beta (Akt/GSK3β) signalling cascade [54]. Increased expression of FOXO3 significantly suppresses myocardial fibrosis and leads to improved myocardial remodeling in atrial fibrillation, as demonstrated in an *in vivo* and *ex vivo* study [55]. *TLR7* in acute myocardial infarction may mediate the response to acute myocardial injury and chronic remodeling by regulating post-infarction scar formation and myeloid-derived inflammatory myocardial infiltration [56]. Based on these premises, it is rational to infer that TMEM173, CTSL, FOXO3, and TLR7 might play active roles in the myocardial fibrosis seen in DCM.

Our lncRNA-mRNA coexpression network analysis identified 4 lncRNAs that displayed particularly strong associations with mRNAs implicated in fibrosis, including *TMEM173*, *CTSL*, *FOXO3*, and *TLR7*. These lncRNAs were identified as follows: lnc-NEK10-3, lnc-KDM4A-2, lnc-PCYOX1-3, and lnc-CDCP2-1 in the form of RNA affected cytoplasmic mRNA stability and translation through epigenetic modification, transcriptional activation/disruption, and intranuclear transport, thereby regulating various signalling pathways [57]. Multiple studies have provided compelling evidence supporting the critical role of lncRNA expression in the progression of myocardial fibrosis in DCM. For instance, in the presence of elevated glucose levels or exposure to interleukin 17 (IL-17), the expression of lncRNA AK081284 exhibited an increase within mouse cardiac fibroblasts. Conversely, the inhibition of IL-17 mitigated the high-glucose-induced upregulation of lncRNA AK081284, resulting in reduced collagen and transforming growth factor 1 beta (TGF-β1) production in cardiac fibroblasts, thereby inhibiting interstitial myocardial fibrosis [58]. By inhibiting the dual specificity phosphatases/extracellular signal-regulated kinase (DUSP5/ERK1/2) axis, lncRNA H19 promotes cardiac fibroblast proliferation and myocardial fibrosis [59]. These findings collectively imply that lncRNAs modulate myocardial fibrosis by regulating pertinent mRNAs. Our findings reveal that lnc-NEK10-3, lnc-KDM4A-2, lnc-PCYOX1-3, and lnc-CDCP2-1 exhibit the most pronounced correlations with the aforementioned fibrosis-associated mRNAs. To the best of our knowl-

edge, no prior studies have documented the involvement of these lncRNAs in myocardial fibrosis associated with DCM. However, our research suggests that these lncRNAs could be critical players in cardiac fibrosis occurring in DCM. Future research aimed at exploring the mechanistic roles and functional significance of these lncRNAs in DCM-associated myocardial fibrosis could provide novel insights into disease diagnosis and intervention strategies.

This study was limited by its small sample size, and the results need validation in further research with multiple-centre population.

In summary, these findings suggest that *SMD11*, *DRG1*, *RPS26*, *EIF2S1*, *UBE3A*, *CEBPZ*, *NUP153*, and *EMD* may serve as central genes implicated in the pathogenesis of DCM. Furthermore, TMEM173, CTSL, FOXO3, and TLR7 were associated with myocardial fibrosis development in diabetic cardiomyopathy. Of note, lnc-NEK10-3, lnc-KDM4A-2, lnc-PCYOX1-3, and lnc-CDCP2-1 demonstrated the strongest correlations with mRNAs linked to myocardial fibrosis, thereby positioning them as potential diagnostic biomarkers and therapeutic targets for the management of DCM cases presenting with myocardial fibrotic changes. The exploration and manipulation of these molecular players hold promise for advancing our understanding of DCM pathogenesis and developing targeted interventions to address its progression, particularly when it is compounded by myocardial fibrosis.

Data availability statement

The Affymetrix Gene Chip data presented in this study are deposited in the Gene Expression Omnibus (GEO), accession number: GSE272275.

Ethics statement

The research involving human participants underwent a thorough evaluation and was granted an exemption from requiring ethical approval by the Institutional Ethics Review Board at Jinan University. The patients gave their written informed consent to take part in the study. Each animal experiment followed the protocols approved by the Medical Ethics Committee of the Jinan University (Ethical approval No. 20210826-29). This study was reported in accordance with ARRIVE guidelines.

Author contributions

Guarantor of integrity of the entire study: J.X.; study concepts: X.D., J.X., and D.C.; study design: X.D., J.X., and D.C.; literature research: X.D.; clinical studies: F.Y.; experimental studies: Z.D., L.Y.; data acquisition: Z.D., L.Y.; data analysis: J.H.; statistical analysis: J.H.; manuscript preparation: X.D.; manuscript editing: D.C.; manuscript review: J.X. All authors read and approved the final manuscript

Funding

This study was supported by the Guangdong Basic and Applied Basic Research Foundation (No. 2021B1515140036), the Scientific Research Project of the Binhaiwan Central Hospital of Dongguan (Nos. 2021010 and 2022004), the Medical Science and Technology Foundation of Guangdong Province (No. A2022150).

Acknowledgments

We thank Xiaoxin Ye of OE Biotech, Shanghai, for her assistance in analysing the gene chip data.

Conflict of interest

The authors declare that they have no competing interests

Supplementary material

Supplementary Figures S1 and S2.

References

1. Lloyd-Jones D, Adams RJ, Brown TM, et al. American Heart Association Statistics Committee and Stroke Statistics Subcommittee. Executive summary: heart disease and stroke statistics--2010 update: a report from the American Heart Association. Circulation. 2010; 121(7): 948–954, doi: 10.1161/CIRCULATIONAHA.109.192666, indexed in Pubmed: 20177011.
2. Sun H, Saeedi P, Karuranga S, et al. IDF Diabetes Atlas: Global, regional and country-level diabetes prevalence estimates for 2021 and projections for 2045. Diabetes Res Clin Pract. 2022; 183: 109119, doi: 10.1016/j.diabres.2021.109119, indexed in Pubmed: 34879977.
3. Pearson-Stuttard J, Bennett J, Cheng YJ, et al. Trends in predominant causes of death in individuals with and without diabetes in England from 2001 to 2018: an epidemiological analysis of linked primary care records. Lancet Diabetes Endocrinol. 2021; 9(3): 165–173, doi: 10.1016/S2213-8587(20)30431-9, indexed in Pubmed: 33549162.
4. Wang M, Li Y, Li S, et al. Endothelial Dysfunction and Diabetic Cardiomyopathy. Front Endocrinol (Lausanne). 2022; 13: 851941, doi: 10.3389/fendo.2022.851941, indexed in Pubmed: 35464057.
5. Dillmann WH. Diabetic Cardiomyopathy. Circ Res. 2019; 124(8): 1160–1162, doi: 10.1161/CIRCRESAHA.118.314665, indexed in Pubmed: 30973809.
6. Jia G, Whaley-Connell A, Sowers JR. Diabetic cardiomyopathy: a hyperglycaemia- and insulin-resistance-induced heart disease. Diabetologia. 2018; 61(1): 21–28, doi: 10.1007/s00125-017-4390-4, indexed in Pubmed: 28776083.
7. Wan A, Rodrigues B. Endothelial cell-cardiomyocyte crosstalk in diabetic cardiomyopathy. Cardiovasc Res. 2016; 111(3): 172–183, doi: 10.1093/cvr/cvw159, indexed in Pubmed: 27288009.
8. Lundbaek K. Diabetic angiopathy: a specific vascular disease. Lancet. 1954; 266(6808): 377–379, doi: 10.1016/s0140-6736(54)90924-1, indexed in Pubmed: 13131862.
9. Asbun J, Villarreal FJ. The pathogenesis of myocardial fibrosis in the setting of diabetic cardiomyopathy. J Am Coll Cardiol. 2006; 47(4): 693–700, doi: 10.1016/j.jacc.2005.09.050, indexed in Pubmed: 16487830.
10. Thorvaldsen JL, Duran KL, Bartolomei MS. Deletion of the H19 differentially methylated domain results in loss of imprinted expression of H19 and Igf2. Genes Dev. 1998; 12(23): 3693–3702, doi: 10.1101/gad.12.23.3693, indexed in Pubmed: 9851976.
11. Zhang EB, Han L, Yin DD, et al. c-Myc-induced, long, noncoding H19 affects cell proliferation and predicts a poor prognosis in patients with gastric cancer. Med Oncol. 2014; 31(5): 914, doi: 10.1007/s12032-014-0914-7, indexed in Pubmed: 24671855.
12. Dykes IM, Emanueli C. Transcriptional and Post-transcriptional Gene Regulation by Long Non-coding RNA. Genomics Proteomics Bioinformatics. 2017; 15(3): 177–186, doi: 10.1016/j.gpb.2016.12.005, indexed in Pubmed: 28529100.
13. Ma H, Hao Y, Dong X, et al. Molecular mechanisms and function prediction of long noncoding RNA. ScientificWorldJournal. 2012; 2012: 541786, doi: 10.1100/2012/541786, indexed in Pubmed: 23319885.
14. Gong C, Maquat LE. lncRNAs transactivate STAU1-mediated mRNA decay by duplexing with 3' UTRs via Alu elements. Nature. 2011; 470(7333): 284–288, doi: 10.1038/nature09701, indexed in Pubmed: 21307942.
15. Cesana M, Cacchiarelli D, Legnini I, et al. A long noncoding RNA controls muscle differentiation by functioning as a competing endogenous RNA. Cell. 2011; 147(2): 358–369, doi: 10.1016/j.cell.2011.09.028, indexed in Pubmed: 22000014.
16. Bai R, Sun M, Chen Y, et al. H19 recruited N 6 -methyladenosine (m 6 A) reader YTHDF1 to promote SCARB1 translation and facilitate angiogenesis in gastric cancer. Chin Med J (Engl). 2023; 136(14): 1719–1731, doi: 10.1097/CM9.0000000000002722, indexed in Pubmed: 37279381.
17. Kong M, Yu X, Zheng Q, et al. Oncogenic roles of LINC01234 in various forms of human cancer. Biomed Pharmacother. 2022; 154: 113570, doi: 10.1016/j.biopha.2022.113570, indexed in Pubmed: 36030582.
18. Wang R, Shiu HT, Lee WY. Emerging role of lncRNAs in osteoarthritis: An updated review. Front Immunol. 2022; 13: 982773, doi: 10.3389/fimmu.2022.982773, indexed in Pubmed: 36304464.

19. Hao Y, Xie Bo, Fu X, et al. New Insights into lncRNAs in Aβ Cascade Hypothesis of Alzheimer's Disease. Biomolecules. 2022; 12(12), doi: 10.3390/biom12121802, indexed in Pubmed: 36551230.
20. Singh DD, Kim Y, Choi SAh, et al. Clinical Significance of MicroRNAs, Long Non-Coding RNAs, and CircRNAs in Cardiovascular Diseases. Cells. 2023; 12(12), doi: 10.3390/cells12121629, indexed in Pubmed: 37371099.
21. Guo Y, Feng X, Wang D, et al. Long Non-coding RNA: A Key Regulator in the Pathogenesis of Diabetic Cardiomyopathy. Front Cardiovasc Med. 2021; 8: 655598, doi: 10.3389/fcvm.2021.655598, indexed in Pubmed: 33889601.
22. Meng L, Lin H, Huang X, et al. METTL14 suppresses pyroptosis and diabetic cardiomyopathy by downregulating TINCR lncRNA. Cell Death Dis. 2022; 13(1): 38, doi: 10.1038/s41419-021-04484-z, indexed in Pubmed: 35013106.
23. Xie R, Fan J, Wen J, et al. LncRNA ZNF593-AS alleviates diabetic cardiomyopathy via suppressing IRF3 signaling pathway. Mol Ther Nucleic Acids. 2023; 32: 689–703, doi: 10.1016/j.omtn.2023.04.025, indexed in Pubmed: 37215148.
24. Zhang M, Gu H, Xu W, et al. Down-regulation of lncRNA MALAT1 reduces cardiomyocyte apoptosis and improves left ventricular function in diabetic rats. Int J Cardiol. 2016; 203: 214–216, doi: 10.1016/j.ijcard.2015.10.136, indexed in Pubmed: 26512840.
25. Piccoli MT, Gupta SK, Viereck J, et al. Inhibition of the Cardiac Fibroblast-Enriched lncRNA Prevents Cardiac Fibrosis and Diastolic Dysfunction. Circ Res. 2017; 121(5): 575–583, doi: 10.1161/CIRCRESAHA.117.310624, indexed in Pubmed: 28630135.
26. Seferović PM, Paulus WJ. Clinical diabetic cardiomyopathy: a two-faced disease with restrictive and dilated phenotypes. Eur Heart J. 2015; 36(27): 1718–27, 1727a, doi: 10.1093/eurheartj/ehv134, indexed in Pubmed: 25888006.
27. Harreiter J, Roden M. [Diabetes mellitus-Definition, classification, diagnosis, screening and prevention (Update 2019)]. Wien Klin Wochenschr. 2019; 131(Suppl 1): 6–15, doi: 10.1007/s00508-019-1450-4, indexed in Pubmed: 30980151.
28. Pang A, Hu Y, Zhou P, et al. Corin is down-regulated and exerts cardioprotective action via activating pro-atrial natriuretic peptide pathway in diabetic cardiomyopathy. Cardiovasc Diabetol. 2015; 14: 134, doi: 10.1186/s12933-015-0298-9, indexed in Pubmed: 26446774.
29. Adeghate E. Molecular and cellular basis of the aetiology and management of diabetic cardiomyopathy: a short review. Mol Cell Biochem. 2004; 261(1-2): 187–191, doi: 10.1023/b:mcbi.0000028755.86521.11, indexed in Pubmed: 15362503.
30. Rubler S, Dlugash J, Yuceoglu YZ, et al. New type of cardiomyopathy associated with diabetic glomerulosclerosis. Am J Cardiol. 1972; 30(6): 595–602, doi: 10.1016/0002-9149(72)90595-4, indexed in Pubmed: 4263660.
31. Guo Q, Zhu Q, Zhang T, et al. Integrated bioinformatic analysis reveals immune molecular markers and potential drugs for diabetic cardiomyopathy. Front Endocrinol (Lausanne). 2022; 13: 933635, doi: 10.3389/fendo.2022.933635, indexed in Pubmed: 36046789.
32. Pant T, Mishra MK, Bai X, et al. Microarray analysis of long non-coding RNA and mRNA expression profiles in diabetic cardiomyopathy using human induced pluripotent stem cell-derived cardiomyocytes. Diab Vasc Dis Res. 2019; 16(1): 57–68, doi: 10.1177/1479164118813888, indexed in Pubmed: 30482051.
33. De Rosa S, Arcidiacono B, Chiefari E, et al. Type 2 Diabetes Mellitus and Cardiovascular Disease: Genetic and Epigenetic Links. Front Endocrinol (Lausanne). 2018; 9: 2, doi: 10.3389/fendo.2018.00002, indexed in Pubmed: 29387042.
34. Meagher P, Civitarese R, Lee X, et al. The Goto Kakizaki rat: Impact of age upon changes in cardiac and renal structure, function. PLoS One. 2021; 16(6): e0252711, doi: 10.1371/journal.pone.0252711, indexed in Pubmed: 34166385.
35. Sharma U, Chakraborty M, Chutia D, et al. Cellular and molecular mechanisms, genetic predisposition and treatment of diabetes-induced cardiomyopathy. Curr Res Pharmacol Drug Discov. 2022; 3: 100126, doi: 10.1016/j.crphar.2022.100126, indexed in Pubmed: 36568261.
36. Fourny N, Lan C, Sérée E, et al. Protective Effect of Resveratrol against Ischemia-Reperfusion Injury via Enhanced High Energy Compounds and eNOS-SIRT1 Expression in Type 2 Diabetic Female Rat Heart. Nutrients. 2019; 11(1), doi: 10.3390/nu11010105, indexed in Pubmed: 30621358.
37. Zhao L, Dong M, Xu C, et al. Identification of Energy Metabolism Changes in Diabetic Cardiomyopathy Rats Using a Metabonomic Approach. Cell Physiol Biochem. 2018; 48(3): 934–946, doi: 10.1159/000491960, indexed in Pubmed: 30036879.
38. Waddingham MT, Edgley AJ, Astolfo A, et al. Chronic Rho-kinase inhibition improves left ventricular contractile dysfunction in early type-1 diabetes by increasing myosin cross-bridge extension. Cardiovasc Diabetol. 2015; 14: 92, doi: 10.1186/s12933-015-0256-6, indexed in Pubmed: 26194354.
39. Tan Yi, Zhang Z, Zheng C, et al. Mechanisms of diabetic cardiomyopathy and potential therapeutic strategies: preclinical and clinical evidence. Nat Rev Cardiol. 2020; 17(9): 585–607, doi: 10.1038/s41569-020-0339-2, indexed in Pubmed: 32080423.
40. Kanamori H, Naruse G, Yoshida A, et al. Morphological characteristics in diabetic cardiomyopathy associated with autophagy. J Cardiol. 2021; 77(1): 30–40, doi: 10.1016/j.jjcc.2020.05.009, indexed in Pubmed: 32907780.
41. Wu W, Liu X, Han L. Apoptosis of cardiomyocytes in diabetic cardiomyopathy involves overexpression of glycogen synthase kinase-3β. Biosci Rep. 2019; 39(1), doi: 10.1042/BSR20171307, indexed in Pubmed: 30237226.
42. Jia G, Hill MA, Sowers JR. Diabetic Cardiomyopathy: An Update of Mechanisms Contributing to This Clinical Entity. Circ Res. 2018; 122(4): 624–638, doi: 10.1161/CIRCRESAHA.117.311586, indexed in Pubmed: 29449364.
43. Packer M. Autophagy-dependent and -independent modulation of oxidative and organellar stress in the diabetic heart by glucose-lowering drugs. Cardiovasc Diabetol. 2020; 19(1): 62, doi: 10.1186/s12933-020-01041-4, indexed in Pubmed: 32404204.
44. Wang L, Cai Y, Jian L, et al. Impact of peroxisome proliferator-activated receptor- on diabetic cardiomyopathy. Cardiovasc Diabetol. 2021; 20(1): 2, doi: 10.1186/s12933-020-01188-0, indexed in Pubmed: 33397369.
45. Xin Z, Ma Z, Jiang S, et al. FOXOs in the impaired heart: New therapeutic targets for cardiac diseases. Biochim Biophys Acta Mol Basis Dis. 2017; 1863(2): 486–498, doi: 10.1016/j.bbadis.2016.11.023, indexed in Pubmed: 27890702.
46. Zhang M, Sui W, Xing Y, et al. Angiotensin IV attenuates diabetic cardiomyopathy suppressing FoxO1-induced excessive autophagy, apoptosis and fibrosis. Theranostics. 2021; 11(18): 8624–8639, doi: 10.7150/thno.48561, indexed in Pubmed: 34522203.
47. Marino F, Scalise M, Salerno N, et al. Diabetes-Induced Cellular Senescence and Senescence-Associated Secretory Phenotype Impair Cardiac Regeneration and Function Independently of Age. Diabetes. 2022; 71(5): 1081–1098, doi: 10.2337/db21-0536, indexed in Pubmed: 35108360.
48. Li Y, Xu Y, Hou Y, et al. Construction and Bioinformatics Analysis of the miRNA-mRNA Regulatory Network in Diabetic Nephropathy. J Healthc Eng. 2021; 2021: 8161701, doi: 10.1155/2021/8161701, indexed in Pubmed: 34840704.
49. Mishra PK. Why the diabetic heart is energy inefficient: a ketogenesis and ketolysis perspective. Am J Physiol Heart Circ Physiol. 2021; 321(4): H751–H755, doi: 10.1152/ajpheart.00260.2021, indexed in Pubmed: 34533402.
50. Li C, Zhang J, Xue M, et al. SGLT2 inhibition with empagliflozin attenuates myocardial oxidative stress and fibrosis in diabetic mice heart. Cardiovasc Diabetol. 2019; 18(1): 15, doi: 10.1186/s12933-019-0816-2, indexed in Pubmed: 30710997.
51. Xu Y, Fang H, Xu Q, et al. LncRNA GAS5 inhibits NLRP3 inflammasome activation-mediated pyroptosis in diabetic cardiomyopathy by targeting miR-34b-3p/AHR. Cell Cycle. 2020; 19(22): 3054–3065, doi: 10.1080/15384101.2020.1831245, indexed in Pubmed: 33092444.
52. Zhang R, Kang R, Tang D. The STING1 network regulates autophagy and cell death. Signal Transduct Target Ther. 2021; 6(1): 208, doi: 10.1038/s41392-021-00613-4, indexed in Pubmed: 34078874.
53. Yan M, Li Y, Luo Q, et al. Mitochondrial damage and activation of the cytosolic DNA sensor cGAS-STING pathway lead to cardiac pyroptosis and hypertrophy in diabetic cardiomyopathy mice. Cell Death Discov. 2022; 8(1): 258, doi: 10.1038/s41420-022-01046-w, indexed in Pubmed: 35538059.
54. Tang Q, Cai J, Shen D, et al. Lysosomal cysteine peptidase cathepsin L protects against cardiac hypertrophy through blocking AKT/GSK3beta signaling. J Mol Med (Berl). 2009; 87(3): 249–260, doi: 10.1007/s00109-008-0423-2, indexed in Pubmed: 19096818.
55. Hu J, Wang X, Cui X, et al. Quercetin prevents isoprenaline-induced myocardial fibrosis by promoting autophagy via regulating miR-223-3p/FOXO3. Cell Cycle. 2021; 20(13): 1253–1269, doi: 10.1080/15384101.2021.1932029, indexed in Pubmed: 34097559.
56. de Kleijn DPV, Chong SY, Wang X, et al. Toll-like receptor 7 deficiency promotes survival and reduces adverse left ventricular remodelling after myocardial infarction. Cardiovasc Res. 2019; 115(12): 1791–1803, doi: 10.1093/cvr/cvz057, indexed in Pubmed: 30830156.
57. Statello L, Guo CJ, Chen LL, et al. Gene regulation by long non-coding RNAs and its biological functions. Nat Rev Mol Cell Biol. 2021; 22(2): 96–118, doi: 10.1038/s41580-020-00315-9, indexed in Pubmed: 33353982.
58. Qi Y, Wu H, Mai C, et al. LncRNA-MIAT-Mediated miR-214-3p Silencing Is Responsible for IL-17 Production and Cardiac Fibrosis in Diabetic Cardiomyopathy. Front Cell Dev Biol. 2020; 8: 243, doi: 10.3389/fcell.2020.00243, indexed in Pubmed: 32351959.
59. Tao H, Cao W, Yang JJ, et al. Long noncoding RNA H19 controls DUSP5/ERK1/2 axis in cardiac fibroblast proliferation and fibrosis. Cardiovasc Pathol. 2016; 25(5): 381–389, doi: 10.1016/j.carpath.2016.05.005, indexed in Pubmed: 27318893.